J|A|C|S

A R T I C L E S

Direct Measurement of the Hyperfine and *g*-Tensors of a Mn(III)−Mn(IV) Complex in Polycrystalline and Frozen Solution Samples by High-Field EPR

Christelle Hureau,[†] Geneviève Blondin,[†] Michèle Cesario,[‡] and Sun Un[*,§]

Contribution from the Laboratoire de Chimie Inorganique, UMR 8613, Institut de Chimie Moléculaire et des Matériaux d'Orsay, Université Paris XI, F-91405 Orsay Cedex, France; Laboratoire de Cristallochimie, Institut de Chimie des Substances Naturelles, UPR CNRS 2301, F-91198 Gif-sur-Yvette, France; and Service de Bioénergétique, DBJC, CNRS-URA 2096, CEA Saclay, F-91191 Gif-sur-Yvette, France

Abstract: The *g*-tensors and hyperfine tensors of the $S = {}^1/_2$ ground state of the mixed valence [LMn(III)-(μ-O)$_2$Mn(IV)L]$^{3+}$ complex (L = *N,N'*-dimethyl-*N,N'*-bis(2-pyridylmethyl)ethane-1,2-diamine) was determined in the solid-state and frozen acetonitrile solution by high-field EPR. Both samples exhibited complex anisotropic temperature behaviors that precluded the use of routine spectrum simulation procedures to extract the spin parameters. To circumvent this problem, the parameters were measured directly by using multifrequency techniques. In the case of the frozen solution, this approach yielded seven of the nine spin parameters with varying uncertainty, the two extreme principal *g*-values, the four hyperfine couplings associated with each of these two *g*-values, and the middle *g*-value. This latter parameter was obtained from a first moment analysis. Unlike simulations, the statistical errors associated with each value could be assigned in a straightforward and rigorous manner. The directly measured *g*-values were different in frozen solution and polycrystalline powder. The temperature dependence of the high-field EPR spectra of the polycrystalline powder revealed a spin−spin interaction between the neighboring binuclear complexes.

Introduction

Synthetic mixed-valence di-μ-oxo Mn(III)−Mn(IV) complexes are the simplest structural and spectroscopic models of polynuclear manganese centers in biological systems, such as those found in photosystem II and manganese catalase. These synthetic systems are characterized by a strongly antiferromagnetic coupling between the two manganese ions resulting in a highly stabilized spin-$^1/_2$ electronic ground state. The conventional 9 GHz electron paramagnetic resonance (EPR) spectrum of these synthetic complexes is a distinct complex 16-line pattern.[1] Such a spectrum has also been observed for the Mn(III)−Mn(IV) oxidation state of manganese catalase.[2] This multiline spectrum reflects the magnetic interaction of the asymmetrically delocalized spin density with the two manganese nuclei ($I = {}^5/_2$). In particular, approximately +2 spins are on the Mn(III) ion, and −1, on the Mn(IV) ion. This leads to two hyperfine couplings that differ by approximately a factor of 2.

This factor of 2 difference leads to the distinct 16-lines pattern. The EPR spectrum of the so-called "S$_2$" oxidation state of the four manganese cluster[3,4] of the PSII is considerably more complicated with more lines and features.[5] This increase in complexity presumably arises from the larger number of manganese ions. For the biological and model systems, much effort has been directed toward accurately determining the hyperfine couplings from which the spin-density distribution can be deduced and, therefore, the electronic wavefunction.[6,7] The Zeeman interaction, the interaction of the electronic spin with the applied magnetic field, has largely been ignored as a source of information.

For conventional microwave excitation frequencies (<35 GHz), the EPR spectra of mixed valence polynuclear manganese centers are dominated by the hyperfine interactions. However, it has been demonstrated that the line shapes of the individual resonances do depend on the anisotropy of the electronic Zeeman interaction, or g-anisotropy, and that simulations of the EPR spectra were improved by taking into account the anisot-

† Institut de Chimie Moléculaire d'Orsay.
‡ Institut de Chimie des Substances Naturelles.
§ Service de Bioénergétique, DBJC.

(1) Cooper, S. R.; Dismukes, G. C.; Klein, M. P.; Calvin, M. *J. Am. Chem. Soc.* **1978**, *100*, 7248−7252.
(2) Khangulov, S. V.; Barynin, V. V.; Antonyuk-Barynina, S. V. *Biochim. Biophys. Acta* **1990**, *1020*, 25−33. Khangulov, S. V.; Barynin, V. V.; Voevodskaya, N. V.; Grebenko, A. I. *Biochim. Biophys. Acta* **1990**, *1020*, 305−310. Fronko, R. M.; Penner-Hahn, J. E.; Bender, C. J. *J. Am. Chem. Soc.* **1988**, *110*, 7554−7555. Haddy, A.; Waldo, G. S.; Sands, R. H.; Penner-Hahn, J. E. *Inorg. Chem.* **1994**, *33*, 2677−2682.
(3) Zouni, A.; Witt, H.-T.; Kern, J.; Fromme, P.; Krauss, N.; Saenger, W.; Orth, P. *Nature* **2001**, *409*, 739−743.
(4) Yachandra, V. K.; Sauer, K.; Klein, M. P. *Chem. Rev.* **1996**, *96*, 2927−2950.
(5) Dismukes, G. C.; Siderer, Y. *Proc. Natl. Acad. Sci. U.S.A.* **1981**, *78*, 274−278.
(6) Peloquin, J. M.; Britt, R. D. *Biochim. Biophys. Acta* **2001**, *1503*, 96−111.
(7) Blondin, G.; Davydov, R.; Philouze, C.; Charlot, M.-F.; Styring, S.; Åkermark, B.; Girerd, J. J.; Boussac, A. *J. Chem. Soc., Dalton Trans.* **1997**, 4069−4074.

ropy of effective *g*-values.[8] However, the contribution of g-anisotropy in conventional EPR spectra is small and difficult to access in any meaningful way.

We and others have exploited the fact that the contribution of g-anisotropy to the EPR spectrum linearly scales with the applied magnetic field and have used high-magnetic field to determine and better characterize the *g*-values of the mixed-valence Mn(III)−Mn(IV) centers.[9,10] The first high-field EPR measurements of g-anisotropies of a number of Mn(III)−Mn(IV) complexes were obtained using 95 and 285 GHz EPR.[9] It was found that g-anisotropies, as defined by $|g_x - g_z|$, of mixed-valence binuclear Mn(III)−Mn(IV) complexes were small ($\Delta g \approx 0.025$). Even at 10 T (285 GHz), the g-anisotropies only started to dominate over the hyperfine couplings. However, it was shown that the g-anisotropy could be determined with reasonable certainty using simulations. The Mn(III)-Mn(IV) g-anisotropies were found to be correlated to the averaged manganese−nitrogen axial bond distances. Recently, the signal arising from the binuclear center in manganese catalase has been detected by 95 GHz EPR.[10] The catalase g-tensor was found to be most similar to the model complex that, like the protein, had a carboxylate bridge between the two manganese ions.[10,11] These initial studies show that the *g*-tensors of the mixed-valence binuclear center are very sensitive to its structure.

We have reexamined a variant of one of the complexes of the previous study[9] with the intent of obtaining the spin parameters with greater accuracy. The complex was crystallized with large tetraphenylborate counterions in an attempt to separate the paramagnetic binuclear centers sufficiently so that it would be possible to obtain hyperfine-resolved spectra using even crystalline samples. The crystallographic structure indeed showed that the centers are well spaced, and we report here the first well-resolved 9 GHz multiline spectra from a solid-state sample. Unexpectedly, we found that both solution and powder samples exhibited nonideal temperature effects that prevented routine simulation procedures from working with any degree of certainty. Rather than relying on simulations, we have used direct methods for measuring several components of hyperfine and g-tensors. Statistical estimates of the errors in the parameters were also determined. This latter point has been underappreciated in many previous studies due to the complexity of determining errors associated with parameters determined from a multidimensional fitting procedure where the model spin Hamiltonian is in itself only an approximation. The ability to measure spin parameters directly is likely to be important for the PSII signal which is more complex and far from an ideal situation with interfering signals that obscure and can potentially distort the multiline structure.

Materials and Methods

Compound Preparation. Reagents and solvents were purchased commercially and used as received. Acetonitrile used for solution studies was distilled before use and dried on an alumina column. The ligand *N,N′*-dimethyl-*N,N′*-bis(2-pyridylmethyl)ethane-1,2-diamine (L) was prepared by following a previously reported procedure.[12]

[LMn(μ-O)₂MnL](BPh₄)₂(ClO₄)·CH₃CN. To a 5 mL aqueous solution of 270 mg (1.0 mmol) of L was added 362 mg (1.0 mmol) of $Mn(ClO_4)_2 \cdot 6H_2O$. The pH was adjusted to 8.5 with $Na_2(CO_3)$ at 5 °C. A solution of hydrogen peroxide (30% w/w) was slowly added with stirring until a precipitate appeared which was collected by filtration and washed with diethyl ether (80% yield). The green powder was then redissolved in acetonitrile, and an excess of sodium tetraphenylborate (2 mmol) was added. The solution was filtered and placed in an ether atmosphere. Crystals of **1**(BPh₄)₂(ClO₄)·CH₃CN (where **1** is [LMn(μ-O)₂MnL]³⁺) suitable for X-ray diffraction studies were obtained, collected by filtration, washed with ether, and dried in air. Anal. Calcd for $C_{82}H_{87}N_9O_6ClB_2Mn_2$: C, 67.39; H, 6.00; N, 8.62; Cl, 2.43; B, 1.48; Mn, 7.52. Found: C, 67.07; H, 6.18; N, 8.72; Cl, 2.65; B, 1.67; Mn, 7.27. IR: ν (cm⁻¹): 3054 (s), 1605 (m), 1577 (m), 1477 (m), 1444 (m), 1425 (m), 1373 (s), 1298 (m), 1262 (s), 1184 (s), 1154 (s), 1092 (w), 1031 (s), 1015 (s), 976 (s), 842 (s), 811 (m), 736 (s), 709 (s), 683 (s), 646 (s), 612 (m), 588 (s), 509 (s), 467 (s), 416 (s). **(Caution: Perchlorate salts of metal complexes with organic ligands are potentially explosive. Only small quantities of these compounds should be prepared and handled behind suitable protective shields.)**

Magnetic Susceptibility Measurements. Magnetic susceptibility data were recorded on an MPMS5 magnetometer (Quantum Design Inc.). The calibration was made at 298 K using a palladium reference sample furnished by Quantum Design Inc. The data were collected over a temperature range of 2−300 K at a magnetic field of 0.1 T and were corrected for diamagnetism.

Crystal Structure of 1(BPh₄)₂(ClO₄)·CH₃CN. ([C₃₂H₄₄N₈-Mn₂O₂](ClO₄)(BPh₄)₂·CH₃CN, M = 1451; monoclinic, space group *Pn*, *a* = 14.678(5) Å, *b* = 11.049(4) Å, *c* = 24.038(6) Å, α = 90°, β = 97.11(2)°, γ = 90°, V = 3868 Å³, T = 293(2) K, Z = 2, F(000) = 1534.) A prismatic dark brown crystal of 0.6 × 0.4 × 0.2 mm³ was mounted on an Enraf−Nonius Kappa-CCD diffractometer. A full sphere of data was collected with Mo Kα radiation (λ = 0.7107 Å) by ϕ-axis rotation with an increment of 1.5° over 360° and 90 s exposure per degree. "Denzingering" was accomplished by measuring each frame twice. Data were analyzed using Kappa-CCD software (Enraf-Nonius, Delft, Netherlands). Cell dimensions were refined with HKL-SCALEPACK, and data reduction was performed with DENZO.[13] The structure was solved by direct methods (SHELX-S86)[14] and was refined on F^2 for all reflections by least-squares methods using SHELXL-93.[15] Hydrogen atoms were included in the calculated positions by using a riding model and were assigned isotropic thermal parameters 1.2 times that of the bound atoms.

Structural data have been deposited with the Cambridge Crystallographic Data Center (CCDC depository number 201748).

(8) Zheng, M.; Khangulov, S. V.; Dismukes, G. C.; Barynin, V. V. *Inorg. Chem.* **1994**, *33*, 382−387. Zheng, M.; Dismukes, G. C. *Inorg. Chem.* **1996**, *35*, 3307−3319. Schäfer, K.-O.; Bittl, R.; Zweygart, W.; Lendzian, F.; Haselhorst, G.; Weyhermüller, T.; Wieghardt, K.; Lubitz, W. *J. Am. Chem. Soc.* **1998**, *120*, 13104−13120.
(9) Policar, C.; Knüpling, M.; Frapart, Y.-M.; Un, S. *J. Phys. Chem. B* **1998**, *102*, 10391−10398.
(10) Schäfer, K.-O.; Bittl, R.; Lendzian, F.; Barynin, V. V.; Weyhermüller, T.; Wieghardt, K.; Lubitz, W. *J. Chem. Phys. B* **2003**, *107*, 1242−1250.
(11) Barynin, V. V.; Whittaker, M. M.; Antonyuk, S. V.; Lamzin, V. S.; Harrison, P. M.; Artymiuk, P. J.; Whittaker, J. W. *Structure* **2001**, *9*, 725−738.

(12) Poussereau, S.; Blondin, G.; Cesario, M.; Guilhem, J.; Chottard, G.; Gonnet, F.; Girerd, J.-J. *Inorg. Chem.* **1998**, *37*, 3127−3132.
(13) Otwinowski, Z.; Minor, W. *Methods in Enzymology*; Academic Press: San Deigo, CA, 1997; Vol. 276, part A, pp 307−326.
(14) Sheldrick, G. M. *Acta Crystallogr., Sect. A* **1990**, *46*, 467−473.
(15) Sheldrick, G. M. *Program for the Refinement of Crystal Structures*; University of Göttingen: Germany, 1993.

EPR. Powder samples were prepared by finely grinding crystals of compound **1**(BPh$_4$)$_2$(ClO$_4$)·CH$_3$CN. To avoid magnetic alignment of crystallites, the polycrystalline powder was suspended in mineral oil and frozen in liquid nitrogen. For the frozen solutions, crystalline sample of **1**(BPh$_4$)$_2$(ClO$_4$)·CH$_3$CN was dissolved in acetonitrile in the presence of 0.1 M tetrabutylammonium perchlorate with a final concentration of approximately 5 mM and frozen in liquid nitrogen and stored at 77 K until use.

Conventional 9 GHz EPR spectra were recorded on a Bruker 200D spectrometer (Rheinstetten, Germany) equipped with an Oxford Instruments (Oxon, England) continuous flow liquid helium cryostat and a temperature control system.

The high-field spectrometer has been described elsewhere.[16] Although the spectrometer used in the present study was similar to that used in the previous study of binuclear complexes, there were several notable differences. A highly stabilized 93–97 GHz microwave synthesizer (ELVA-1, St. Peterburg, Russia) was used instead of a free running Gunn diode. The microwave frequency was stable to less than 1 kHz and was reproducibly adjustable to within this accuracy in steps of 100 MHz. In conjunction to a frequency tripler (Radiometer Physics, Meckenheim, Germany), a frequency doubler from the same manufacturer was also extensively employed. The magnet system (Oxford Instruments, Oxon, England) was calibrated and capable of reproducible linear sweeps (see below). The stability and reproducibility of both the microwave generation and magnetic field were crucial to the direct measurement technique used in this study. All spectra were obtained under nonsaturating conditions.

For the high-field EPR measurements, the magnetic field was calibrated using manganese-doped magnesium oxide standard having an isotropic g-values of 2.001 01 and isotropic hyperfine coupling of 0.008 69 T (243 MHz, 81.3 × 10^{-4} cm^{-1}).[17] The line width of the hyperfine lines were limited by the modulation field used, typically 0.25 mT. The isotropic g-value, isotropic hyperfine coupling, and zero-field coupling were obtained by fitting the spectra using third-order perturbation equations of de Wijn and von Balderen[18] and standard conjugate gradient minimization techniques.[19] Each of the six lines was identical in width and amplitude indicating that second-order dependencies on the zero-field parameter were negligible at these magnetic fields. The calibration procedure was repeated using microwave frequencies between 280.50 and 289.50 GHz at 1.50 GHz intervals for the 10 T region and between 187.00 and 193.00 GHz at 1.00 GHz intervals for the 6 T region. The g-values obtained from the fits were used to generate a calibration curve. Comparison of the simulation and experimental spectra indicated a highly linear sweep. Any nonlinear effects were below the 0.25 mT modulation-limited line width. In fact, field positions of the six hyperfine lines determined by simulation differed from the experiment by no more than 0.15 mT. The correlation between the magnetic field obtained from the manufacturer-calibrated power supply and experimental measured field was also highly linear over the two narrow ranges

measured. However, the correlation curves for the 6 and 10 T regions differed significantly indicating nonlinear behavior over a larger magnetic field range. Over the duration of the experiments, the total calibration procedure was carried out twice, and numerous single-point measurements were also used to validate the reproducibility of the calibration curves.

Theory of Measurements. The basis of our study was the direct measurement of the electronic Zeeman. To describe the theoretical basis for such measurements, we consider the specific case where the magnetic field, B, is along the g_x direction of the principal axis system of the binuclear manganese center g-tensor. As previously mentioned, the EPR spectra are governed by the Zeeman interaction and the two manganese hyperfine couplings. When the magnetic field is sufficiently large so that the Zeeman interaction is dominant, as is the case for all of the high-field measurements describe in the following, the spin Hamiltonian reduces to

$$\hat{H} = g_x\beta B\hat{S}_x + \hat{S}_x(A_{III,xx}\hat{I}_{III,x} + A_{III,xy}\hat{I}_{III,y} + A_{III,xz}\hat{I}_{III,z}) + \hat{S}_x(A_{IV,xx}\hat{I}_{IV,x} + A_{IV,xy}\hat{I}_{IV,y} + A_{IV,xz}\hat{I}_{IV,z}) \quad (1)$$

This equation can be readily transformed into a much simpler form[20]

$$\hat{H} = g_x\beta B\hat{S}_Z + A'_{III,x}\hat{S}_Z\hat{I}_{III,Z} + A'_{IV,x}\hat{S}_Z\hat{I}_{IV,Z} \quad (2)$$

where the electronic spin quantization axis is along the magnetic field direction. This equation can be readily solved yielding a relationship between the microwave frequency, ν, and the applied magnetic field B:

$$h\nu = g_x\beta B + |A'_{III,x}|m_{III} + |A'_{IV,x}|m_{IV} \quad (3)$$

where the m_{III} and m_{IV} are the nuclear spin quantum numbers. This leads to an EPR spectrum centered at g_x with the hyperfine structure determined by the absolute value of the two effective hyperfine couplings $|A'_{III,x}|$ and $|A'_{IV,x}|$ along the g_x direction. If the hyperfine and g-tensors are collinear in this direction, $A'_{III,x}$ and $A'_{IV,x}$ are simply equal to $A_{III,xx}$ and $A_{IV,xx}$, respectively.

Therefore, for a fixed orientation of the magnetic field with respect to the g-axis system, the change in the field position of a given hyperfine line is predicted to be linearly dependent on the microwave excitation frequency. A plot of the microwave frequency as a function of the quantity βBh^{-1} should yield a line with a slope equal to g_x and zero magnetic field intercept $|A'_{III,x}|m_{III} + |A'_{IV,x}|m_{IV}$. Since to a first approximation $A'_{III,x}$ is equal to $-2A'_{IV,x}$, the lowest-field hyperfine line would have an intercept of $(5|A'_{III,x}|/2 + 5|A'_{IV,x}|/2)$ and the second of $(5|A'_{III,x}|/2 + 3|A'_{IV,x}|/2)$. For the two highest-field hyperfine lines, the results are identical but opposite in sign. Therefore, the measurement of the first two hyperfine lines should, in principle, yield $|A'_{III,x}|$ and $|A'_{IV,x}|$. The above description is true for any orientation of the magnetic field with respect to the g-axis system. In the general case, g_x is replaced by

$$g_{eff} = \sqrt{(g_x^2\cos^2\varphi + g_y^2\sin^2\varphi)\sin^2\theta + g_z^2\cos^2\theta} \quad (4)$$

where θ and φ are the azimuthal and longitudinal angles describing the orientation of the magnetic field with respect to

(16) Un, S.; Dorlet, P.; Rutherford, A. W. *Appl. Magn. Reson.* **2001**, *21*, 341–361.
(17) Burghaus, O.; Plato, M.; Rohrer, M.; Möbius, K.; MacMillan, F.; Lubitz, W. *J. Phys. Chem.* **1993**, *97*, 7639–7647.
(18) de Wijn, H. W.; van Balderen, F. *J. Chem. Phys.* **1967**, *46*, 1381–1387.
(19) Press, W. H.; Flannery, B. P.; Tenkolski, S. A.; Vetterling, W. T. *Numerical Recipe*; Cambridge University Press: New York, 1986.
(20) (a) Abragam, A.; Bleaney, B. *Electron Paramagnetic Resonance of Transition Ions*; Dover Publications: New York, 1970. (b) Taylor, P. C.; Baugher, J. F.; Kriz, H. M. *Chem. Rev.* **1975**, *75*, 203–240.

the *g*-axis system. The effective hyperfine coupling constants can be expressed in a similar manner.[20]

In our previous study, we have shown that at 285 GHz the g-anisotropy of binuclear Mn(III)−Mn(IV) complexes in frozen solution constitutes about 45% of the total spectra extent. In these cases, the lowest and highest hyperfine lines correspond purely to the g_x and g_z orientations, respectively, and measurement of their absolute resonant magnetic field as a function of microwave frequency will yield their corresponding *g*-values and magnitude of the two hyperfine couplings. This means that six out of the nine spin parameters (3 *g*-values and 6 hyperfine values) can be obtained directly by the multifrequency measurements.

The complexity of the middle region of the spectrum precludes any possibility of direct measurement of the third *g*-value. However, it is possible to estimate the middle *g*-value by the application of moments analysis.[21] In nuclear magnetic resonance, it has been shown that the first moment of a chemical shift powder pattern is equal to the isotropic value of the chemical shift tensor.[21] The first moment is given by the following equation, where *B* is the magnetic field and *f*(*B*) is the line shape function.

$$\int B \, f(B) \, \mathrm{d}B$$

By analogy, the first moment of the high-field EPR spectra would be the field position corresponding to the isotropic *g*-value, g_{iso}, defined by $^1/_3(g_x + g_y + g_z)$. This relationship is approximately independent of the presence of spin couplings, since these interactions are inherently symmetrical at such high fields and do not contribute to the first moment.

Results

Crystal Structure. The asymmetric unit **1**(BPh$_4$)$_2$(ClO$_4$)· CH$_3$CN consisted of one dinuclear [Mn(III)(μ-O)$_2$Mn(IV)] complex, two tetraphenylborate anions and one perchlorate anion, together with one cocrystallized acetonitrile solvent molecule (Figure 1). The structure was very similar to that previously reported for crystals containing only perchlorate counterions.[22] The ligand assumed the usual cis-α conformation. The axial Mn−N distances were distinctly longer for one of the two manganese ions characteristic of a Jahn−Teller distortion at the Mn(III) center. These Mn(III)−N bond lengths of 2.165 Å were longer than those in the structure containing only prechlorate anions (2.135 Å).[22] This elongation was attributed to crystal packing effects of the tetraphenylborate anions. In addition, the presence of the bulky tetraphenylborate anions led to a greater separation of the di-Mn-di-μ-oxo entities. On a large scale, the dinuclear Mn(III)−Mn(IV) complexes were organized into chains (Figure 1). Within a chain, the complexes were related by a translation along the crystallographic *b*-axis with the MnO$_2$-Mn units nearly coplanar to each other. The separation between MnO$_2$Mn units within a chain was 11.05 Å. The closest distance between units on different chains was 11.90 Å. Perusal of the crystallographic database for other dinuclear [Mn(III)(μ-O)$_2$-Mn(IV)] compounds where the Mn ions have an [N$_4$O$_2$]
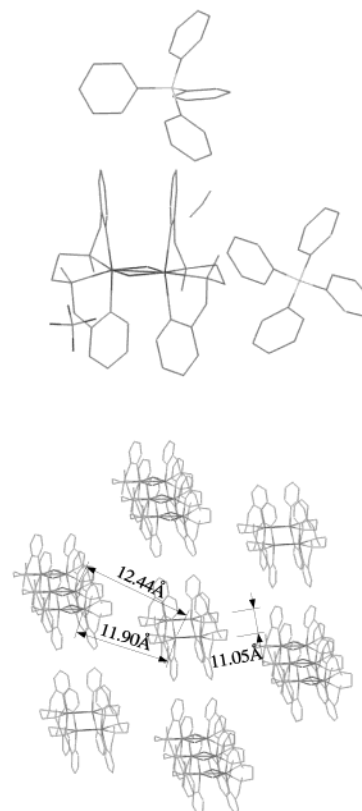
(21) (a) Vanderhart, D. L.; Gutowsky, H. S. *J. Chem. Phys.* **1968**, *49*, 261−271. (b) Slichter, C. P. *Principles of Magnetic Resonance*; Springer-Verlag: Berlin, 1978.
(22) Glerup, J.; Goodson, P. A.; Hazell, A.; Hazell, R.; Hodgson, D. J.; McKenzie, C. J.; Michelsen, K.; Rychlewska, U. *Inorg. Chem.* **1994**, *33*, 4105−4111.

Figure 1. Structure of **1**(BPh$_4$)$_2$(ClO$_4$)·CH$_3$CN. (Top) The asymmetric unit is composed of a binuclear manganese core, two tetraphenylborate anions and one perchlorate anion and one acetonitrile molecule. (Bottom) The manganese complexes form chains within which the Mn(III)−Mn(IV) cores are related by a simple translation and are coplanar. The separation between the binuclear cores on the same chain is 11.05 Å and 11.90 Å on different chains.

coordination sphere[23] indicated that the shortest intermolecular metal−metal distances were between 8.12 and 10.51 Å with an average separation of 9.16 Å. The 11.05 Å separation was indeed significantly larger.

Magnetic Susceptibility Measurements. The molar magnetic susceptibility χ_M of a powder sample of **1**(BPh$_4$)$_2$(ClO$_4$)· CH$_3$CN was measured as a function of the temperature *T*. The data were consistent with strongly antiferromagnetically coupled high-spin Mn(III) ($S_{III} = 2$) and Mn(IV) ($S_{IV} = ^3/_2$) ions. The best fit was obtained with $J = -310$ cm^{-1} using the van Vleck formula and the Heisenberg−Dirac−van Vleck Hamiltonian $-J\mathbf{S_{III}} \cdot \mathbf{S_{IV}}$. This value is in agreement with the -320 cm^{-1} exchange interaction reported for **1**(ClO$_4$)$_3$·3H$_2$O.[22] Such a large negative *J* value leads to a highly stabilized $S = ^1/_2$ electronic ground state. Moreover, this is the only populated spin level below 50 K, even at 10 T. Therefore, the EPR spectra reflect only this $S = ^1/_2$ ground state.

9 GHz EPR Spectroscopy. The conventional 9 GHz EPR frozen solution spectrum of **1** in acetonitrile is shown in Figure 2. The well-resolved signature 16-line spectrum of an [Mn(III)-(μ-O)$_2$Mn(IV)]$^{3+}$ core was observed centered at *g* = 2 and spread over a range of approximately 0.120 T. Superimposed on the solution spectrum is the spectrum of a polycrystalline

(23) Nineteen structures were found in the CDCC database with the following accession codes: FEBKUS, FOGHAK, GAMFEF, GEPSUP, GIXKON, HEWJEY, HEWJOI, HIRMEA, JOJQUU, KEZKUV, KEZLAC, MARROM, SAWYEU, SEJXUA, SIBZUY, WABFIO, YEMCIC, ZAXNER, and ZUKHES.
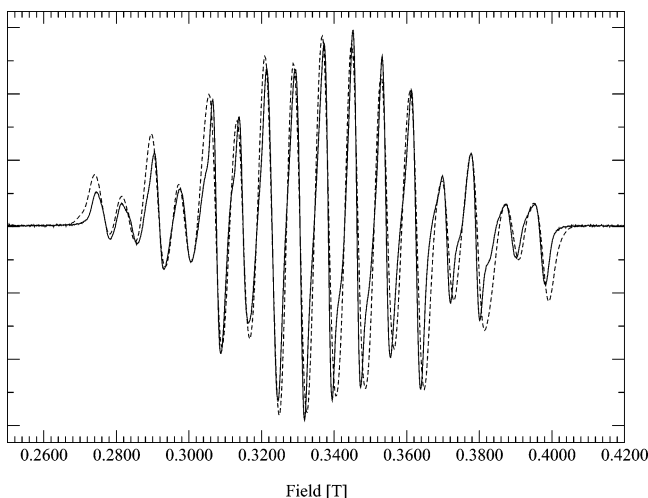
Figure 2. Frozen solution (solid) and polycrystalline powder (dashed) spectra (9 GHz) of **1**(BPh$_4$)$_2$(ClO$_4$)·CH$_3$CN.
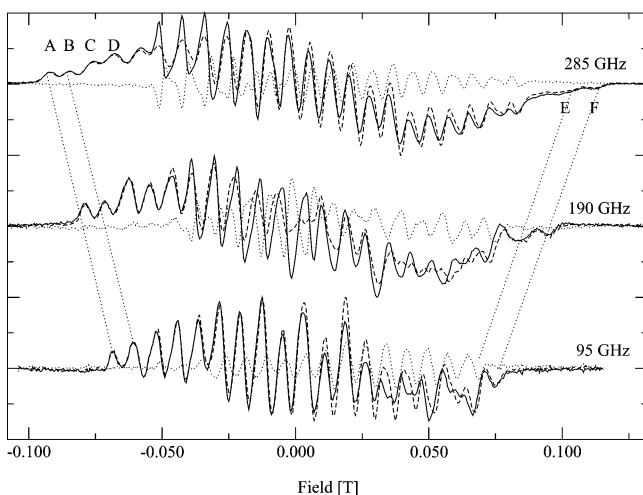
Figure 3. HF-EPR solution spectra of **1**(BPh$_4$)$_2$(ClO$_4$)·CH$_3$CN recorded at 95, 190, and 285 GHz. Zero magnetic field offset is equivalent to a *g*-value of 1.994. Solid-line traces are spectra at 4.2 K, dashed ones are spectra at 10.0 K after Boltzmann scaling, and dotted ones are the 4.2 − 10.0 K difference spectra.

sample of **1**(BPh$_4$)$_2$(ClO$_4$)·CH$_3$CN. The two spectra were nearly identical. As far as we are aware, this is the first observation of a well-resolved 16-line spectrum from a polycrystalline sample of a Mn(III)−Mn(IV) sample. This was initially attributed to the presence of two bulky tetraphenylborate anions per dinuclear manganese complex that induced a greater separation between the paramagnetic centers. The individual hyperfine features in the powder spectrum were only slightly broader than in the solution spectrum. The peak-to-trough widths were approximately 3.0 mT in the frozen solution and 4.0 mT in the polycrystalline sample. The field positions of the 16 lines were identical.

Frozen Solution HF-EPR Spectra. The 4 K frozen solution EPR spectra of **1** recorded at 95, 190, and 285 GHz are shown Figure 3. The spectra exhibited better hyperfine resolution than in our previous study.[9] The overall spectral width increased with microwave frequency: 0.144 T at 95 GHz, 0.170 T at 190 GHz, and 0.204 T at 285 GHz. This variation was directly related to the anisotropy of the Zeeman interaction. If one assumes that the extent of the 9 GHz spectrum was purely due to hyperfine

interactions, then the difference between the spectral extent of the 285 and 9 GHz gives directly the g-anisotropy contribution to the 285 GHz spectrum. The g-anisotropy of **1** estimated in this way was 0.018, in agreement with the previous estimate for this complex.[9] Thus, 45% of the 285 GHz spectral width was due to g-anisotropy. For the 9 GHz spectrum (Figure 2), this anisotropy corresponds to about 3.0 mT. Hence, the line widths at this low frequency were nearly completely determined by the g-anisotropy.

The frozen solution spectra were also recorded at 10 K. When the intensities of the 4 and 10 K spectra were corrected for temperature (Figure 3), it became evident that the loss in intensity was greater at the center than at the wings. This could not be attributed solely to contaminant Mn(II) ions. The 10 − 4 K difference spectrum was strikingly similar to the 9 GHz spectrum (see Supporting Information for addition information). Similar temperature differences were also observed at 190 and 95 GHz (Figure 3). At 95 GHz, the difference spectrum contained exactly 16 lines centered at $g = 1.9902 \pm 0.0005$. These observations suggested the presence of an unresolved anisotropic temperature-dependent contribution to the inhomogeneous line width. Direct measurements of the relaxation rates using high magnetic field pulse EPR techniques would be required to better characterize this behavior.

This nonideal temperature dependence posed a dilemma with respect to simulations, since most standard simulation methods implicitly assume that all spins are identical and ideal with respect to temperature. We used a more direct and simple method to circumvent such limitations and directly measured the Zeeman and hyperfine interactions. The field positions of various features of the spectra were monitored as a function of the excitation frequency. The hyperfine features chosen for the measurements were the four lowest-field hyperfine lines (labeled A−D in Figure 3) and the two highest (labeled E−F). The multifrequency data suggested that these six lines used in these measurements originated from unique orientations: the first four lowest-field lines from the g_x direction and the two highest-field from the g_z. This orientation selection was a direct consequence of the higher resolution in g-anisotropy made possible by the use of high magnetic fields.

Figure 4 summarizes the results from the multifrequency measurements. Data were obtained from six different frequencies in the 190 GHz range and nine in the 285 GHz region. At several particular frequencies, data from several spectra were used to assess errors in the measurements. The g_x and g_z values obtained from the linear regression analysis along with the statistical errors are given in Table 1. The average of the four g_x values was $2.001\,90 \pm 0.000\,10$. The greatest deviations were observed for the two g_z hyperfine lines. Both of the high-field hyperfine features were broader than the low-field ones, and the maxima were poorly defined, especially in the 190 GHz spectra. The g_z value determined from the two measurements was $1.984\,44 \pm 0.000\,61$.

In the case of the four low-field features, it was possible to plot the zero magnetic field intercepts obtained from the linear regression analysis of the multifrequency measurements as a function of the nuclear spin quantum number m_{IV} (Figure 5). Under ideal conditions, such a plot should be linear with a slope of $-|A'_{IV,x}|$ and a zero-intercept (i.e., $m_{IV} = 0$) corresponding to $5|A'_{III,x}|/2$. In fact, the zero magnetic field intercepts given
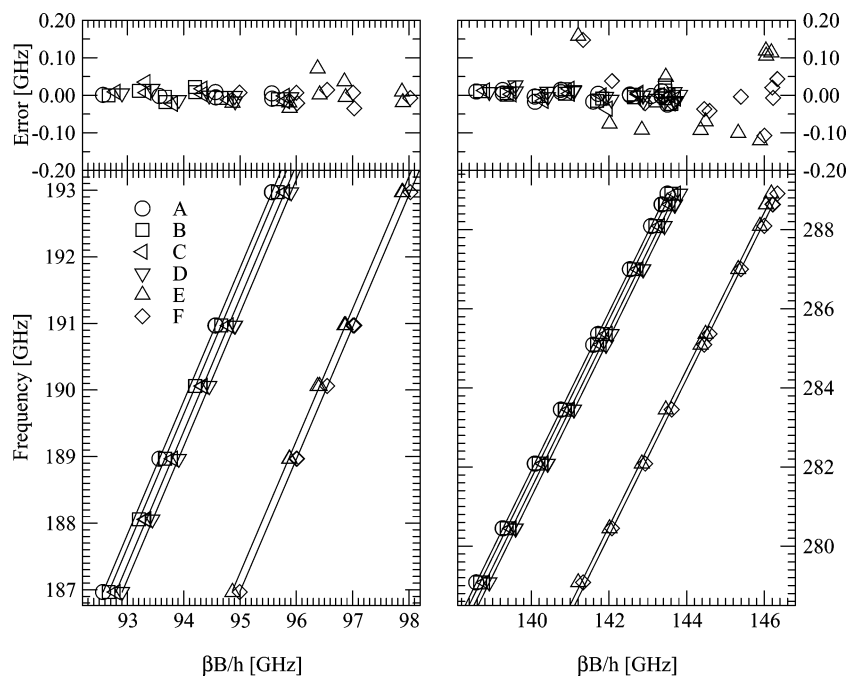
Figure 4. Resonant magnetic field positions of the hyperfine features in a frozen solution sample of **1** as a function of microwave frequency. The labels correspond to those in Figure 3. The magnetic field values have been multiplied by β/h (13.996 242 GHz/T). Although the plots have been divided into the 180 and 285 GHz domains, the linear regression analyses treated data from both domains as a single set. The upper panels show the fit residuals.

Table 1. Summary of the Line Regression Analysis of the Solution Multifrequency Measurements[d]

hyperfine line[a]	g	zero magnetic field intercept $|A'_{III}|m_{III} + |A'_{IV}|m_{IV}$	zero magnetic field intercept at 9 GHz[b,c]
A	2.001 85	1.660	1.740
	(0.000 09)	(0.012)	
B	2.001 79	1.471	1.549
	(0.000 10)	(0.012)	
C	2.001 97	1.193	1.327
	(0.000 12)	(0.015)	
D	2.001 97	0.971	1.126
	(0.000 10)	(0.012)	
E	1.984 02	1.228	1.384
	(0.000 07)	(0.092)	
F	1.984 85	1.585	1.606
	(0.000 04)	(0.053)	

[a] See Figure 3 for letter designation. [b] Calculated as $(\nu - g\beta B/h)$ with g = 1.9931. [c] Uncertainity: ±0.084 GHz (see text). [d]Zero magnetic field intercepts are expressed in GHz. Uncertainties are in parentheses

in Table 1 did form a straight line. Regression analysis yielded $|A'_{III,x}| = 0.436 \pm 0.020$ GHz and $|A'_{IV,x}| = 0.234 \pm 0.011$ GHz. As expected, the Mn(III) effective hyperfine coupling constant $|A'_{III,x}|$ was found to be about twice as large as the one of the Mn(IV) $|A'_{IV,x}|$.[24] The $|A'_{III,x}|$ was slightly lower and the $|A'_{IV,x}|$ was higher than those previously reported.[9] The relatively large uncertainty in the g_z data and the lack of more than two points made any further analysis difficult. Based on the two zero-field intercepts, the hyperfine constants were found to be 0.357 ± 0.075 and 0.277 ± 0.075 GHz. This simple treatment assigned the larger hyperfine value to $|A'_{IV,z}|$ which was highly unlikely. However, it should be noted that these values were nearly within the statistical uncertainty limits of each other and those previously obtained by simulation, 0.351 and 0.223 GHz for $|A'_{III,z}|$ and $|A'_{IV,z}|$, respectively.[9]

As a further test of the analysis of high-field data, the relative field positions of the first four and last two hyperfine features in the 9 GHz spectrum were calculated assuming an isotropic
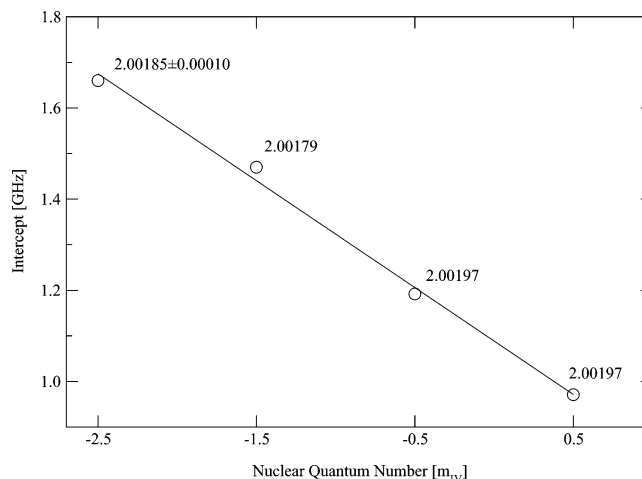

Figure 5. Intercepts obtained from Figure 4 as a function of the Mn(IV) nuclear spin quantum number (see text for details). The points are labeled by the g-values given in Table 1. The best fit line corresponds to 1.089-(±0.02) $-$ 0.234(±0.011) m_{IV} yielding $|A'_{III,x}| = 0.436$ GHz and $|A'_{IV,x}| = 0.234$ GHz.

g of 1.9931 (see below) (Table 1). These values should ideally be the same as the zero magnetic field intercepts determined from the multifrequency analysis. The upper bound for the error in defining the field position of the 9 GHz hyperfine lines (Figure 2) was estimated from the fact that the line width is determined by the g-anisotropy (3 mT at 0.3 T or 0.084 GHz). The outer peaks A, B, and F were in reasonably good agreement with those obtained from the 190 and 285 GHz measurements. The agreement for the inner three peaks (C, D, E) was poorer but no more than twice the estimated error.

To determine the g_y value, we applied first moment analysis to 95, 190, and 285 GHz data obtained at 4 and 10 K. First, a

(24) Bencini, A.; Gatteschi, D. *Electron Paramagnetic Resonance of Exchange Coupled Systems*; Springer-Verlag: New York, 1990.
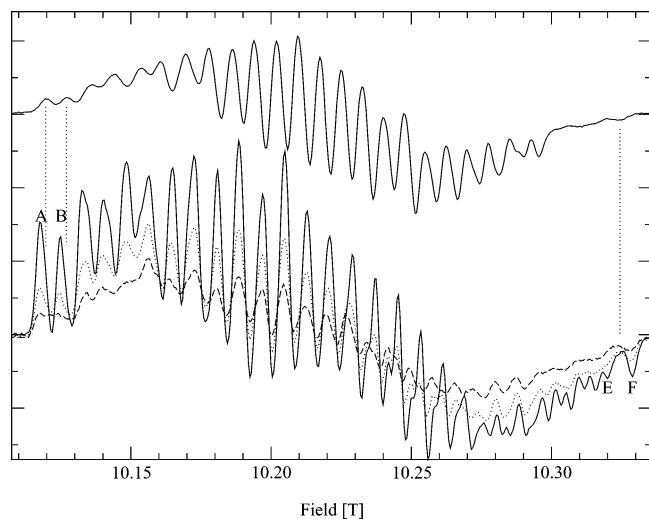
Figure 6. EPR spectra (285 GHz) of a powder sample of **1**(BPh$_4$)$_2$-(ClO$_4$)·CH$_3$CN at 3 K (solid, lower trace), 8 K (dotted), and 15 K (dashed). The frozen solution spectrum is also shown for reference (solid, upper trace).

Figure 7. EPR spectrum (190 GHz) a powder sample of **1**(BPh$_4$)$_2$-(ClO$_4$)·CH$_3$CN obtained at 4 K (solid) and 8 K (dashed). The arrows mark the positions of two of the resonances that grow with increasing temperature.

quadratic polynomial was used to correct the baseline of the spectra that were then integrated. Even after such a baseline correction, in about half of the cases, the value of the integral immediately at the start and end of the signal differed significantly. This is most likely due to slow random drifting of the baseline during data acquisition. Of those spectra that behaved ideally, the first moment was calculated. The values were: 1.9941 ± 0.0002 (seven spectra) at 285 GHz, 1.9923 ± 0.0002 (six spectra) at 190 GHz, and 1.9926 ± 0.0004 (two spectra) at 95 GHz. The lack of agreement between the results obtained at the three frequency regions was not completely unanticipated. Contributions to the first moment from nonideal temperature behavior and contaminating Mn(II) signals increased with increasing microwave frequency. Interestingly, the first moments of the 285 GHz spectra obtained at 4 and 10 K (Figure 3) were essentially identical. The nonideal temperature effects discussed above were nearly centered about the estimated g_{iso} and are roughly symmetrical about the center. In this case, these thermally induced changes would not alter the first moment. It is also for this reason that the lower frequency data are less affected by Mn(II) signals since the centers of signals in terms of absolute magnetic field arising from the binuclear and Mn(II) centers are closer at lower frequencies. The corresponding g_y-values of complex **1** were 1.9960, 1.9906, and 1.9915, for the 285, 190, and 95 GHz measurements, respectively. Since the two lower frequency measurements are affected less by systematic error, the two lower values, which are statistically nearly identical, are likely to be closer to the actual value. In summary, of the seven spin parameters that were accessible for direct measurement, the g_y-value was only determined to modest accuracy and the $|A'_{III,x}|$ and $|A'_{IV,x}|$ were determined rather poorly. The large statistical uncertainties of these latter two values were indicative of the limits of the measurement techniques when the resonances are broad and poorly resolved. By contrast, the remaining four spin parameters of frozen solution sample were determined with good accuracy.

Polycrystalline Powder HF-EPR Spectra. The polycrystalline powder HFEPR spectra of **1**(BPh$_4$)$_2$(ClO$_4$)·CH$_3$CN also exhibited a distinct temperature behavior (Figures 6 and 7). The Curie-like decrease in amplitude with increase in temperature
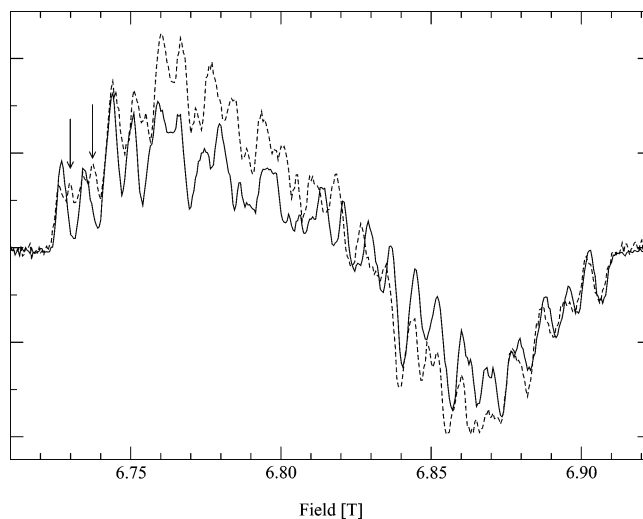
was accompanied by an apparent loss in resolution due to the appearance of additional resonances. This was particularly evident in the g_x region of the 190 GHz spectra (Figure 7) where two additional partial resolved peaks were clearly present at 8 K but not at 4 K. These peaks were displaced approximately +4 mT relative to the corresponding peaks at 4 K and achieved equal amplitude with the latter at about 8 K at 190 GHz and 15 K at 285 GHz. These temperature effects appeared to be anisotropic with greater influence on the g_x and g_y portions of the spectra.

Multifrequency measurements were performed on the polycrystalline sample at 4.2 K, but no measurements were made on the high temperatures resonances due to poor spectral resolution. The measurements on the two dominant lowest- (labeled A and B) and highest-field (labeled E and F) hyperfine features of the 4.2 K spectra are summarized in Figure 8 and the regression analysis in Table 2. The deviations from the linear fit were essentially the same as those determined for the solution measurements. The spin parameters obtained from the regression analysis of the third lowest peak (data not shown) differed significantly from those of the two lowest-field lines with deviations that were also significantly larger. The first moment analysis of the 190 and 285 GHz spectra obtained at 4 K did not differ significantly. The analysis yielded an isotropic g-value of 1.9945 ± 0.0010 and a g_y-value of 1.9968. The first moment analysis of the 12 K 285 GHz data yielded a slightly lower isotropic g-value of 1.9936 ± 0.0007. This correlated with the appearance of the additional hyperfine features (Figures 6 and 7). From the differences in the zero magnetic field intercepts (Table 2), $|A'_{III,x}|$ was estimated to be 517 ± 0.022 GHz, $|A'_{IV,x}|$ 206 ± 0.022 GHz, $|A'_{III,z}|$ 0.474 ± 0.027 GHz, and $|A'_{IV,z}|$ 0.236 ± 0.027 GHz. The $|A'_{III,x}|$ value appeared to be considerably larger than that for solution samples (see below). In contrast to the solution values, $|A'_{IV,z}|$ was indeed smaller than $|A'_{III,z}|$ by a factor of 2.

Discussion

The high-field EPR spectra of complex **1**, in frozen solution and as a polycrystalline powder, exhibited nonideal temperature dependences. In solution, the relative difference between the
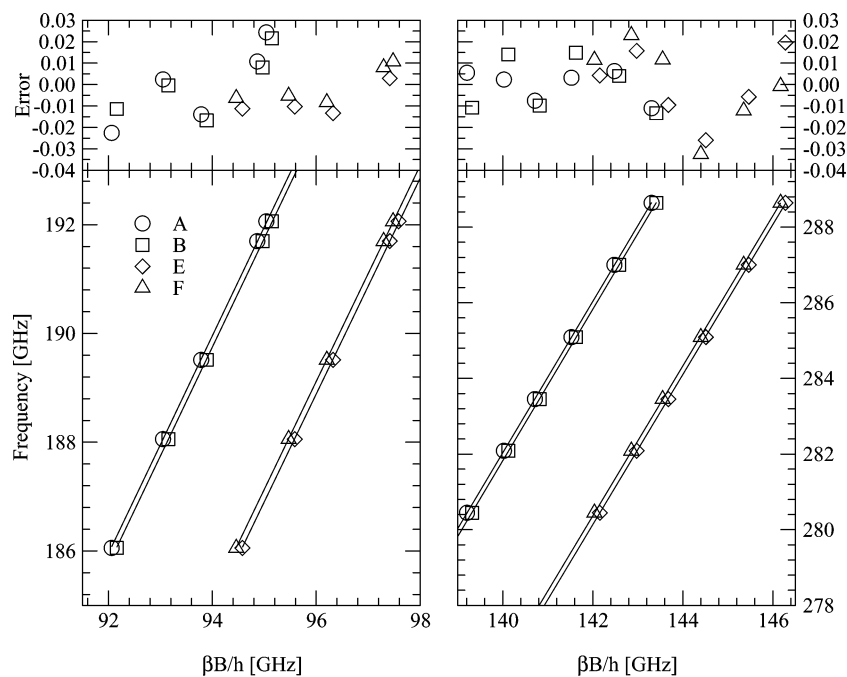
Figure 8. Resonant magnetic field positions of the hyperfine features in a polycrystalline powder sample of **1**(BPh₄)₂(ClO₄)·CH₃CN and difference between the best-fit line and the experimental data points. The labels correspond to those in Figure 6. The magnetic field values have been multiplied by 13.996 242 GHz/T. Although the plots have been divided into the 190 and 285 GHz domains, the linear regression analyses treated data from both domains as a single set.

Table 2. Summary of the Line Regression Analysis of the Polycrystalline Multifrequency Measurements Performed at 4 K[b]

hyperfine line[a]	g	zero magnetic field intercept $|A'_{III}|m_{III} + |A'_{IV}|m_{III}$
A	2.001 58 (0.000 17)	1.808 (0.021)
B	2.001 57 (0.000 18)	1.602 (0.022)
E	1.983 58 (0.000 20)	1.304 (0.025)
F	1.983 63 (0.000 23)	1.540 (0.029)

[a] See Figure 6 for letter designation. [b] Zero magnetic field intercepts are expressed in GHz. Uncertainties are in parentheses.

spectra obtained at 4 and 10 K was a 16-line spectrum. It can be shown directly from eqs 3 and 4 that such a 16-line difference spectrum can only arise from a set of molecules with very similar orientations with respect to the applied magnetic field. The unique temperature dependence of these magnetically orientation selected molecules is presumably due to anisotropic relaxation.[25] The polycrystalline powder sample was quite different. A second set of resonances grew with temperature suggesting the presence of an excited state. In both cases, proper simulations would require a phenomenological or first-principal model of the temperature dependences. Although this might be possible for the polycrystalline powder (see below), a model for the frozen solution spectra would be difficult since the physical origins of the nonideal behavior are not at all understood. The direct measurements of the electronic Zeeman and hyperfine interactions, based on eqs 3 and 4, avoided this problem. The applicability of this approach to the frozen solution and polycrystalline powder samples is demonstrated by the highly linear correlations that were observed over a 95−285 GHz range. The use of high magnetic fields to resolve the g-anisotropy is what made this method possible.

The presence of anisotropic relaxation in the solution spectra of complex **1** has potentially important implications for the study of similar complexes including biological systems. Such non-

ideal anisotropic effects could exist in other systems, including biological ones. In the absence of g-anisotropy resolution, as with conventional 9 GHz EPR spectroscopy, the presence of anisotropic relaxation would not be readily obvious. However, such effects will lead to distortions in the shapes of 16 hyperfine lines. Since, simulation of 9 GHz EPR data depend on the line shapes to obtain information on hyperfine and g-anistropies,[8] simple simulation strategies may not yield correct spin parameters and techniques that measure spin parameters directly, such as ENDOR, which are more preferable.[26]

Although little is known about the underlying cause for anisotropic relaxation behavior in frozen solution, the nature of the excited state observed in polycrystalline powder samples can be readily deduced from the crystal structure. The crystal structure shows that a binuclear manganese core is surrounded by eight others that are all within 13 Å. The closest are two that reside on the same chain at a distance of 11 Å. Beyond the eight, the next nearest are more than 15 Å away. Hence, weak intermolecular magnetic interactions between the cores are not unexpected.

The temperature behavior can be understood by considering a pair of binuclear manganese cores that are magnetically coupled. We have examined the effects of high magnetic field on a similar spin-coupled pair in photosystem II.[27] Such a spin coupling results in a triplet-like ($S = 1$) three level system with relative energies of $-g\beta H$, 0, and $+g\beta H$ (assuming that the

(25) Orientation selection effects due to anisotropic relaxation have been observed for organic radicals; for example, see: Un, S.; Atta, M.; Fontecave, M.; Rutherford, A. W. *J. Am. Chem. Soc.* **1995**, *117*, 10713−10719. Rohrer, M.; Gast, P.; Möbius, K.; Prisner, T. F. *Chem. Phys. Lett.* **1996**, *259*, 523−530.

(26) Randall, D. W.; Sturgeon, B. E.; Ball, J. A.; Lorigan, G. A.; Chan, M. K.; Klein, M. P.; Armstrong, W. H.; Britt, R. D. *J. Am. Chem. Soc.* **1995**, *117*, 11780−11789. Peloquin, J. M.; Campbell, K. A.; Randall, D. W.; Evanchik, M. A.; Pecoraro, V. L.; Armstrong, W. H.; Britt, R. D. *J. Am. Chem. Soc.* **2000**, *122*, 10926−10942.

(27) Dorlet, P.; Boussac, A.; Rutherford, A. W.; Un, S. *J. Phys. Chem. B* **1999**, *103*, 10945−10954.

Zeeman energy is much larger than the spin–spin coupling). At temperatures lower than that corresponding to the Zeeman energy (285 GHz = 14 K and 190 GHz = 9 K), only the lowest level is populated and only one of the two allowed transitions is observable. At temperatures comparable to the Zeeman energy, the middle sublevel will become populated, leading to the appearance of the second transition. This is essentially what was observed experimentally for the polycrystalline sample (Figures 6 and 7). If the spin–spin interaction is dipolar and therefore anisotropic, the relative positions of the two transitions will be field dependent. The fact that the additional resonances were less apparent in high-field regions of the spectra than the low-field portion was consistent with this anisotropic character of the magnetic dipolar coupling.[28] One can also obtain an estimate of interaction energy using the point dipole approximation. The separation between the two transitions of the triplet-like system within this approximation is given by[29]

$$\Delta = \frac{3\mu_0 g^2 \beta^2}{8\pi r^3}(1 - 3\cos^2\Omega) = \frac{2.779 \text{ mT Å}^3}{r^3}(1 - 3\cos^2\Omega)$$

The maximum size of this splitting ($\Omega = 0$) for a spin separation of 11 Å is about −2.1 mT in field units. The maximum spacing between the low and high temperature resonances appeared to be about 4 mT. The underestimation of the dipolar coupling was not too surprising considering that there was another spin within 11 Å and six others only slightly further away.

The presence of spin–spin interactions also accounted for the differences in the zero magnetic field intercepts observed between the solution and polycrystalline samples. The intercepts for peaks A and B (see Table 2) in polycrystalline powder were offset by +0.148 and +0.131 GHz, respectively, relative to the corresponding peaks in the frozen solution (see Table 1). In the absence of spin–spin coupling, this shift indicated that $|A'_{\text{III},x}|$ was about 0.056 GHz or, in field units 2 mT, larger in the powder. If the 4 mT spin–spin interaction is taken into account, then peaks A and B in the powder spectrum are predicted to be shifted by 2 mT by the interaction. Consequently, $|A'_{\text{III},x}|$ would be essentially the same in solution as in the solid. By contrast, the zero magnetic field intercepts for peak E in the polycrystalline powder and frozen solution spectra were statistically the same, as were those for peak F. This further reinforced the notion that the spin–spin interaction was anisotropic.

Although the observed temperature dependence of the polycrystalline powder HFEPR spectra of **1** was consistent with the presence of spin–spin interactions, it was clear why such an interaction was not detected in 9 GHz spectrum. Fournel and co-workers[30] have shown that, even in the presence of spin–

spin interaction, only a single line is observed if the isotropic component (exchange) of the coupling is much larger than the difference in the Zeeman energies of the two individual spins and the anisotropic component (dipolar) is much smaller than both. If the Zeeman energy difference is dominant, then a doublet is predicted. The maximum difference in the Zeeman energy between two binuclear manganese cores in polycrystalline samples of **1** is simply $|g_x - g_z|\beta Bh^{-1}$ or 2.63 GHz at 10 T and 0.08 GHz at 0.3 T. If one assumes that the 4 mT (0.122 GHz) spin–spin coupling is essentially isotropic, then it seems plausible that at high field a doublet is observed while at low field a singlet is seen. However, the apparent anisotropic effect of the high temperature resonances argues against this possibility. Another possible explanation is that at 9 GHz there is sufficient exchange narrowing to average the spin interaction.[24] This implies that the comparable resolution of the polycrystalline powder and frozen solution 9 GHz EPR spectra is due to exchange narrowing rather than to the greater separation of the manganese cores induced by the large tetraphenylborate counterions. Further work is needed to clarify this issue.

This study also presented us with the first opportunity to compare the g-anisotropy in the solid and frozen solution. The g_x- and g_z-values were lower by about 2.5×10^{-4} and 8.0×10^{-4}, respectively, in the frozen solution compared to the crystals, leading to a greater g-anisotropy (defined by $|g_x - g_z|$) in the solid state. In our previous study[9] on frozen solution samples, we demonstrated that the Mn(III)–Mn(IV) g-anisotropy could be linearly correlated to the average of the four axial Mn–N bond lengths measured on crystals obtained using perchlorate anions. Hence, it is likely that bond distance changes upon dissolution cause both values to shift in the same direction by unequal amounts resulting in a change in the g-anisotropy. However, as mentioned above, the average Mn–N$_{\text{axial}}$ value is significantly larger in **1**(BPh$_4$)$_2$(ClO$_4$)·CH$_3$CN (2.165 Å) than in **1**(ClO$_4$)$_3$·H$_2$O (2.135 Å), and it is not clear how this change in bond length will affect the correlation which we have established. Further investigation on the correlation between the g-anisotropies measured in the solid state and structure of Mn(III)–Mn(IV) complexes is currently underway.

Multifrequency high-field EPR experiments offer an elegant alternative way to determine the spin parameters. The procedure developed here is solely based on the resonant magnetic field values. Such an analysis relies only on the assumptions inherent to the spin Hamiltonian with which the spin system is modeled and not on details of the signal intensities. In contrast to the multiparameter fittings using simulations, error analysis of such measurements is straightforward. This is to our knowledge the first time that hyperfine and g-tensors have been assessed without resorting to spectral simulation.

Supporting Information Available: The effect of temperature on the solution spectrum of **1** and demonstration of the use of the first moment to determine the isotropic g-value. This material is available free of charge via the Internet at http://pubs.acs.org.

(28) For a more detailed calculation of dipolar couplings, one would need to include all of the near neighbors and take into account the fact that each spin arises from exchange-coupled pairs. (See: Bertrand, P.; More, C.; Guigliarelli, B.; Fournel, A.; Bennett, B.; Howes, B. *J. Am. Chem. Soc.* **1994**, *116*, 3078−3086.)

(29) (a) Abragam, A. *Principles of Nuclear Magnetism*; Clarendon Press: Oxford, 1970. (b) Dorlet, P.; Di Valentin, M.; Babcock, G. T.; MacCracken, J. L. *J. Phys. Chem. B* **1998**, *102*, 8239−8247.

(30) Fournel, A.; Gambarelli, S.; Guigliarelli, B.; More, C.; Asso, M.; Choteau, G.; Hille, R.; Bertrand, P. *J. Chem. Phys.* **1998**, *109*, 10905−10913.

JA035153B